Journal of Materials Chemistry B

RSC Publishing

PAPER

View Article Online
View Journal | View Issue

Biomimetic mineralization of calcium carbonate mediated by a polypeptide-based copolymer†

Cite this: *J. Mater. Chem. B*, 2013, **1**, 841

Wenjie Zhu, Jiaping Lin,* Chunhua Cai and Yingqing Lu

Received 28th September 2012
Accepted 30th November 2012

DOI: 10.1039/c2tb00182a

www.rsc.org/MaterialsB

A novel copolymer, β-cyclodextrin-*b*-poly(L-glutamic acid) (β-CD-*b*-PLGA), was synthesized by ring-opening polymerization and subsequent hydrolysis reaction. The β-CD-*b*-PLGA copolymer possesses an oligosaccharide β-CD segment and a polypeptide PLGA segment, with chemical structure resembling natural glycoprotein. The copolymers were applied in regulating the crystallization of calcium carbonate. The effects of the concentration of copolymers and calcium ions were systemically investigated. Various morphologies, including rhombohedra, rod, pseudo-dodecahedra and rosette-like structures, were obtained by adjusting the polymer and Ca^{2+} concentrations of the initial solution. Investigation of the pseudo-dodecahedra growth mechanism indicates that the copolymers mediate amorphous calcium carbonate formation initially, and then regulate the meso-scale self-assembly of $CaCO_3$ subunits. The morphology variation is influenced by the binding of β-CD-*b*-PLGA chains on specific crystal faces combined with the steric repulsive force of β-CD-*b*-PLGA chains.

1 Introduction

It is widespread in biological systems that living organisms synthesize inorganic minerals with complex shapes, hierarchical structures and fascinating properties. Biomineralization is regulated by the cooperation of soluble and insoluble organic components in biological systems.[1] However, the exact mechanism of the interaction between organics and minerals is difficult to explore because the organic components are often structurally complex and difficult to individually isolate from the biominerals.[2] Recently, increasing attention has been given to the biomimetic synthesis of inorganic materials by using various biopolymers and synthetic polymers to explore the fundamental mechanism in biomineralization.[3]

Calcium carbonate ($CaCO_3$) has been of considerable interest because it is one of the most abundant biominerals and used industrially in vast quantities. Hydrophilic polymers, including proteins, polysaccharides and glycoproteins, exist in $CaCO_3$ biominerals and guide the development of the mineral phase.[4] Acidic groups (carboxylate, sulfate, phosphate, *etc.*) in these copolymers could bind Ca^{2+} and crystal faces to control the nucleation and growth of $CaCO_3$.[5,6] Among the biomineral polymers, glycoprotein which comprises of protein segment and covalently attached oligosaccharide chains has received increasing interest due to its effect in the nucleation and growth of crystallization.[7–10] Takagi *et al.* studied the effects of a glycoprotein aggregate of fish otolith matrix and its separate components on $CaCO_3$ crystallization *in vitro*. It was found that the aggregate and the separated components induced different polymorphs and morphologies of $CaCO_3$ crystals under the same conditions.[8] Addadi *et al.* extracted glycoproteins from sea-urchin spines and cleaved the glycoproteins to several fractions, and studied their respective effects on $CaCO_3$ crystallization. The result shows that the polysaccharide moieties as well as the proteins are involved in certain types of interactions with calcite crystals.[9] Mcgrath *et al.* studied the mineralization of $CaCO_3$ in the presence of acidic glycoproteins isolated from adult spines of the sea urchin *Evechinus chloroticus*. It was found that the cleaved oligosaccharides provide a similar growth environment for the $CaCO_3$ as the parent glycoproteins, while the deglycosylated protein does not produce this effect.[10] Despite these observations, the roles of glycoproteins in biomineralization are still far from fully understood due to their complex components and complicated three-dimensional structures.

Inspired by biomineralization process, various synthetic and natural polymers which have a simple structure have been applied in bio-inspired crystallization. Polysaccharides including pectin, κ-carrageenan, and sodium alginate have been utilized for directing the $CaCO_3$ growth, and intriguing hollow crystals were obtained.[11] Because proteins in biominerals often contain acidic amino acid residues, to mimic the protein-mediated biomineralization, acidic polypeptides which can be synthesised by living polymerization are usually used as

Shanghai Key Laboratory of Advanced Polymeric Materials, State Key Laboratory of Bioreactor Engineering, Key Laboratory for Ultrafine Materials of Ministry of Education, School of Materials Science and Engineering, East China University of Science and Technology, Shanghai 200237, China. E-mail: jlin@ecust.edu.cn; Fax: +86-21-64251644; Tel: +86-21-64253370

† Electronic supplementary information (ESI) available: GPC traces of β-CD-*b*-PBLG, thermal analysis of the $CaCO_3$ sample and $CaCO_3$ crystals controlled by CG2, CG3, β-CD and PLGA. See DOI: 10.1039/c2tb00182a

the crystallization modifier.[12–15] Guo and Yu *et al.* prepared various kinds of porous $CaCO_3$ spheres by using poly(ethylene glycol)-*b*-poly(aspartic acid) as a crystal growth modifier.[13] In recent work, we studied the influence of a thermo-responsive polymer, poly(*N*-isopropyl acrylamide)-*b*-poly(L-glutamic acid), on the crystallization of $CaCO_3$ and $BaCO_3$.[14,15] By tuning the temperature, we obtained rosette-like calcite in the unimer solution and aragonite fibers in the polymer micelle solution in the $CaCO_3$ crystallization.[14] It is anticipated that a type of copolymers, which comprises both polypeptide and sugar moiety, can be applied as a model compound for imitating glycoprotein-controlled mineralization.

To better understand the glycoprotein-controlled mineralization, we design and construct a simple model by utilizing a novel copolymer, β-cyclodextrin-*b*-poly(L-glutamic acid) (β-CD-*b*-PLGA), as the $CaCO_3$ crystallization modifier. The β-CD is a common cyclic oligosaccharide, which is a truncated conical molecule with a hollow cavity constituted by seven glucopyranoside units. The copolymer can be considered as a simple model of glycoprotein since the two segments resemble oligosaccharide and protein respectively. It was discovered that the copolymers have remarkable effects on the control of $CaCO_3$ mineralization. A series of calcite morphologies, including rhombohedra, rods, rosettes and pseudo-dodecahedrons, were obtained by adjusting the concentration of the polymer and calcium ion. The mechanism underlying the polymer-mediated crystallization behavior was elucidated.

2 Experimental section

2.1 Materials

β-CD was purchased from Sinopharm Chemical Reagent Co., Ltd., and used after drying in a vacuum oven for 24 hours. *p*-Toluenesulfonyl chloride (*p*-TSCl) was purified by standard procedures. Ethylenediamine (EDA) and *N*,*N*′-dimethylformamide (DMF) were dried over 4 Å molecular sieves for at least 24 h and vacuum distilled before use. Deionized water (DIW) was made in a Millipore Super-Q Plus Water System to a level of 18.2 MΩ cm resistance. γ-Benzyl-L-glutamate–*N*-carboxyanhydride (BLG–NCA) was synthesized by the reaction of γ-benzyl-L-glutamate with triphosgene according to the procedures reported in the literature.[16] $CaCl_2$, $(NH_4)_2CO_3$ and other reagents were of analytical grade and used without further purification. All glassware (glass bottles and small pieces of glass substrates) for the crystallization experiments was cleaned and sonicated in ethanol for 5 min. It was then rinsed with DIW, further soaked in a H_2O–HNO_3(65%)–H_2O_2 (1 : 1 : 1, v/v/v) solution, and then rinsed with DIW. Afterward, it was dried in air with acetone. A dialysis bag (Membra-cel, 3500 molecular weight cutoff) was provided by Serva Electrophoresis GmbH.

2.2 Synthesis of the polymer

Synthesis of mono[6-*O*-(*p*-toluenesulfonyl)]-β-cyclodextrin (6-OTs-β-CD). Mono[6-*O*-(*p*-toluenesulfonyl)]-β-cyclodextrin (6-OTs-β-CD) was prepared by the reaction of *p*-TSCl with β-CD in alkaline aqueous solution according to the method reported in the literature.[17] ^{1}H NMR (500 MHz, DMSO-d_6): $\delta = 7.75$ (d, H^2), $\delta = 7.43$ (d, H^2), $\delta = 5.86$–5.61 (m, H^{14}), $\delta = 4.89$–4.73 (d, H^6), $\delta = 2.43$ (s, H^3) ppm.

Synthesis of mono[6-(2-aminoeythylamino)-6-deoxy]-β-cyclodextrin (EDA-β-CD). EDA-β-CD was prepared by heating 6-OTs-β-CD (2 g) in excess anhydrous ethylenediamine (15 mL) at 70 °C for 7 h.[18] After the reaction was completed, the mixture was allowed to cool to room temperature, and then, 50 mL of cold acetone were added. The precipitate was repeatedly dissolved in 10 mL of water–methanol mixture, and poured into 50 mL of acetone several times for the removal of unreacted EDA. Finally, the sample obtained was dried at 50 °C for 3 days in a vacuum oven. ^{1}H NMR (500 MHz, D_2O): $\delta = 5.01$ (s, H^7), $\delta =$ 4.01–3.88 (m, H^{28}), $\delta = 3.67$–3.45 (m, H^{14}), $\delta = 2.86$–2.76 (m, H^2) ppm; IR (KBr): 3345 cm^{-1} (s, OH), 2928 cm^{-1} (w, CH_2), 1030 cm^{-1} (s, C–OH).

Synthesis of β-cyclodextrin-*b*-poly(γ-benzyl-L-glutamate). β-Cyclodextrin-*b*-poly(γ-benzyl-L-glutamate) (β-CD-*b*-PBLG) was synthesized by ring-opening polymerization of BLG–NCA, initialized by the primary amino group of EDA-β-CD. In a typical procedure, EDA-β-CD (0.2 g) and BLG–NCA (1.6 g) were dissolved in DMF separately in two dry bottles. Then they were mixed in a dry three-neck round-bottom flask. The reaction was performed at room temperature in nitrogen atmosphere. The concentration of BLG–NCA was fixed at ~5%. After 72 h of stirring, the mixture was dialyzed against deionized water and lyophilized to get β-CD-*b*-PBLG powder. The ^{1}H NMR spectra are provided in Fig. S1 in the ESI.† ^{1}H NMR (500 MHz, DMSO-d_6): 7.32 ($Ar–H_{PBLG}$), 5.04 (CH_{2PBLG}), 4.48 ($H_{β\text{-}CD}$-1), 3.72–4.17 ($OH_{β\text{-}CD}$), 3.33 (CH_{PBLG}), 1.75–2.74 ($H_{β\text{-}CD}$-2, $H_{β\text{-}CD}$-3, $H_{β\text{-}CD}$-4, $H_{β\text{-}CD}$-5, $H_{β\text{-}CD}$-6).

Synthesis of β-cyclodextrin-*b*-poly(L-glutamic acid). β-Cyclodextrin-*b*-poly(L-glutamic acid) (β-CD-*b*-PLGA) block copolymers were prepared by hydrolyzation of β-CD-*b*-PBLG with potassium hydroxide (KOH). As a brief, 1 g β-CD-*b*-PBLG was suspended in 50 mL tetrahydrofuran (THF). Then an aqueous solution of KOH (3 mol equiv. with respect to the benzyl group) was added to the suspension. After 4 h of stirring, the mixture was neutralized with hydrochloric acid and dialyzed against water to remove organic solvent and other small molecule impurities. A white powder was obtained by lyophilizing the dialyzed solution. The benzyl groups were completely removed after hydrolyzation as indicated by the disappearance of methylene proton peak (5.04 ppm) from the ^{1}H NMR spectra (Fig. S1†).

2.3 Mineralization

The β-CD-*b*-PLGA solution was first prepared by directly dissolving β-CD-*b*-PLGA in basic solution. In a typical procedure, 50 mg β-CD-*b*-PLGA was dissolved in 40 mL DIW in a 100 mL bottle. 11.1 mg (0.1 mmol) $CaCl_2$ was also added as the calcium source of $CaCO_3$. Then, the pH value of the solution was carefully adjusted to 9.0 (±0.1) by adding a small quantity of 1 M hydrochloric acid (HCl) or 1 M sodium hydroxide (NaOH). The final solution volume was fixed at 50 mL by adding water. After then, the solution was filtered by using a 0.22 μm Millipore to remove impurities. The synthesis of $CaCO_3$ was performed by the gas diffusion method

described by Addadi and co-workers.[9] The reaction vessel with 10 mL β-CD-*b*-PLGA solution was covered with parafilm punched with 4 holes, and then placed in a closed desiccator at room temperature (22 ± 1 °C). A glass bottle containing crushed ammonium carbonate, also covered with pierced parafilm, was placed in the same desiccator as the source of CO_2. The glass slides were taken out from the vessels at different times, rinsed with distilled water and allowed to dry in the air for further analysis. All experiments were repeated several times.

2.4 Measurements

^{1}H Nuclear Magnetic Resonance (^{1}H NMR). ^{1}H NMR spectra measurements were performed on a Bruker Avance 550 spectrometer using dimethyl sulfoxide-d_6, D_2O or other deuterated solvent and tetramethylsilane as an internal standard at room temperature.

Gel Permeation Chromatography (GPC). The molecular weight and polydispersity of β-CD-*b*-PBLG copolymers were measured by GPC (Polymer Lab, PL-GPC50 plus) using PBLG with narrow molecular weight distribution as standard, performed in LiBr/DMF solution.

Field Emission Scanning Electron Microscopy (FE-SEM). The crystals on the glass wafers were observed by scanning electron microscopy (SEM) (HITACHI-4800) operated at an accelerating voltage of 10 kV. Before the observation, the samples were sputtered with gold.

High-Resolution Transmission Electron Microscopy (HR-TEM) and Selective Area Electronic Diffraction (SAED). The HR-TEM image and SAED were performed on a JEM-2100F HR-TEM operated at an accelerating voltage of 200 kV. The crystal in the glass bottle was collected and dispersed in water. And then, the sample was transferred to a copper grid with carbon film and dried in air before the observation. SAED was also performed using this instrument.

Atomic Force Microscopy (AFM). The surface of the crystals on the glass wafers was directly observed by a multimode atomic force microscopy (XE-100, PSIA), using the non-contact mode.

X-ray Diffraction (XRD). XRD was used to analyze the crystalline structure. The XRD patterns were recorded on Rigaku D/Max-2550V with Cu Kα radiation in the range $2\theta = 10$–80°.

Fourier Transform Infrared Spectra (FT-IR). For FT-IR analysis, the samples were pressed with KBr into pellets. The spectra of the samples were recorded on a Nicolet 5700 FT-IR spectrometer in transmission mode.

Thermogravimetry analysis (TG). TG was performed with a thermogravimetric analyzer (NETZSCH STA 409 PC/PG) at a heating rate of 10 °C min^{-1} from room temperature to 800 °C under nitrogen flow.

Conductivity measurement. The interactions between polymers and Ca^{2+} were tested by using conductivity measurement. At a fixed Ca^{2+} concentration of 50 mM, the concentration of polymers was varied from 1.0 to 5.0 g L^{-1}. The conductivities for the polymer and polymer–$CaCl_2$ hybrid systems were measured with a DDSJ-308A conductometer (Shanghai REX Instrument Factory) at 25 °C.

3 Results and discussion

3.1 Synthesis and characterization of β-CD-*b*-PLGA

The synthesis of β-CD-*b*-PLGA block copolymers was illustrated in Scheme 1. The initiator EDA-β-CD, which has only one amino group as the active initiating site, was prepared by modifying β-CD with two reaction steps, etherifying with *p*-TSCl and aminolysis with an excess amount of EDA. Then β-CD-*b*-PBLG diblock copolymer was synthesized *via* ring-opening polymerization of BLG–NCA initiated by primary amino groups of EDA-β-CD. The length of PBLG segment was controlled by adjusting the feeding ratio of BLG–NCA to macroinitiator. Finally, the β-CD-*b*-PLGA was obtained after alkaline hydrolysis for deprotection of benzyl ester.

The number-average molecular weight (M_n) and the polydispersity index of the molecular weight distribution (PDI = M_w/M_n) were measured by gel permeation chromatography (GPC) using DMF/LiBr as eluent. GPC traces of the β-CD-*b*-PBLG block copolymer samples with various PBLG lengths are presented in Fig. S2 (see ESI†). Each sample shows a monomodal distribution, indicating a successful synthesis of copolymers. The PDIs are 1.19, 1.24 and 1.27 for β-CD-*b*-$PBLG_{55}$, β-CD-*b*-$PBLG_{36}$, and β-CD-*b*-$PBLG_{17}$ respectively (the subscripts refer to the PBLG repeating units). The hydrolysis products β-CD-*b*-PLGA copolymers are denoted as CG1, CG2 and CG3 respectively. The detailed information is provided in Table 1. The β-CD-*b*-PLGA copolymers can be directly dissolved in water without using any NaOH, indicating that the copolymers have a good solubility.

3.2 Effect of polymer concentration on morphosynthesis of $CaCO_3$ crystals

The calcium carbonate crystallization was performed by using a gas diffusion method. The gas diffusion method is a commonly used method for mineralization.[9] In such a method, the ammonium carbonate decomposes slowly and releases CO_2, which further gradually diffuses into the solution, generates CO_3^{2-} and reacts with $CaCl_2$ to form $CaCO_3$. In such processes, the supersaturation in the solution is not very high. Therefore, the additives can control the crystallization properly. As is well known, rhombohedral shaped calcite crystals consisting of six

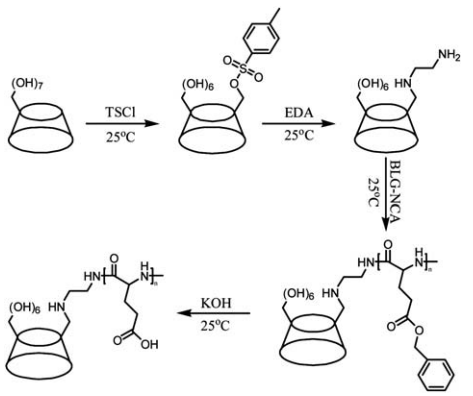

Scheme 1 Synthetic route for the β-CD-*b*-PLGA copolymers.

Table 1 Characteristics of β-CD-*b*-PLGA copolymers

Sample	Copolymer[a]	M_n[a]	PDI[b]
CG1	β-CD-*b*-$PLGA_{55}$	8316	1.19
CG2	β-CD-*b*-$PLGA_{36}$	5730	1.24
CG3	β-CD-*b*-$PLGA_{17}$	3311	1.27

[a] The number-average molecular weights (M_n) were calculated by GPC of the precursor β-CD-*b*-PBLG using PBLG with narrow molecular weight distribution as standard, LiBr/DMF as eluent. [b] Polydispersity indexes (PDI), M_w/M_n (M_w is the weight-average molecular weight and M_n is the number-average molecular weight) of the precursor β-CD-*b*-PBLG are determined by GPC.

{104} faces can be produced under equilibrium conditions in the absence of polymers.[6] The CG1 was first presented as the modifier of $CaCO_3$ crystallization. The concentration of Ca^{2+} was fixed at 2 mM. The effect of polymer concentration on the mineralization was investigated by adjusting the polymer concentration from 0.001 to 2.0 g L^{-1}. XRD was used to identify the crystalline phase of the as-prepared samples (Fig. 1). For all samples prepared, the XRD pattern exhibits the characteristic reflection of calcite (*d*-spacings/Å: 3.87, 3.04, 2.84, 2.50, 2.29; corresponding to *hkl*: 012, 104, 006, 110, and 113 respectively). The evolution of $CaCO_3$ morphology as the polymer concentration varied was displayed in Fig. 2. Fig. 2a shows the SEM images of $CaCO_3$ crystals after 3 days of reaction in the presence of 0.001 g L^{-1} polymer solution. The $CaCO_3$ products consist almost entirely of rhombohedra structures, which are similar to typical calcite rhombohedra crystals formed in the absence of polymers. The magnified image in the inset shows the etching pits in {104} faces and truncated edges between the faces. At a CG1 concentration of 0.003 g L^{-1}, the truncated edges can be seen more obviously (Fig. 2b). When the concentration of CG1 further increases to 0.01 g L^{-1}, the morphology of $CaCO_3$ crystals changes to entire rods (Fig. 2c). The rods range from 16 to 24 μm in length and from 8 to 10 μm in width. A similar structure can also be produced in CG1 copolymer solution with the concentration ranging from 0.01 to 0.8 g L^{-1}. Fig. 2d shows

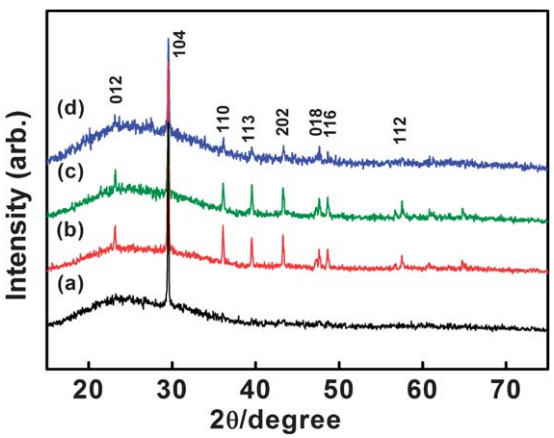

Fig. 1 XRD pattern of $CaCO_3$ samples obtained in the presence of CG1 with various of polymer concentrations, (a) 0.001, (b) 0.01, (c) 0.1, (d) 2.0 g L^{-1}. The concentration of Ca^{2+} is 2 mM.

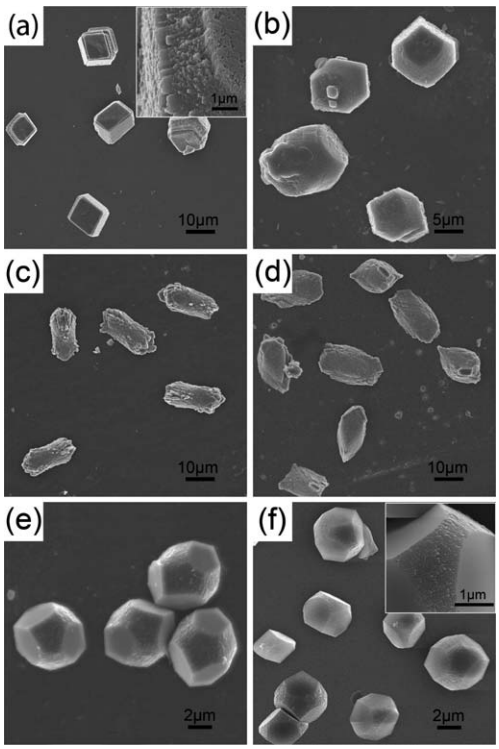

Fig. 2 SEM images of $CaCO_3$ crystals obtained in the presence of CG1 with various polymer concentrations, (a) 0.001, (b) 0.003, (c) 0.01, (d) 0.3, (e) 1.0, (f) 2.0 g L^{-1}. The concentration of Ca^{2+} is 2 mM.

the sample prepared in 0.3 g L^{-1} polymer solution. The rods elongated along the *c*-axis indicating that the polymers express nonspecific inhibition of growth in the envelope of planes {*hk*0}. This is because the carbonate ions align almost perpendicular to the {*hk*0} planes and acidic polymers can easily interact with the crystal planes in this orientation.[19] In this case, {104} faces can only partially be expressed at the tips of a rod crystal.

As the concentration of CG1 was increased to 1.0 and 2.0 g L^{-1}, calcite crystals with a pseudo-dodecahedral shape were produced, as shown in Fig. 2e and f. The crystals have a relatively uniform size, about 6–8 μm. Each pseudo-dodecahedron contains six smooth and six coarse faces. However, the coarse faces cannot be viewed as real faces since they are highly curved. From the magnified image, we can find that the curved faces show a nanogranular surface structure (Fig. 2f, inset). The six rough faces could be indexed as {011} faces.[20] The pseudo-dodecahedral shapes, which are characterized by their barrel-shaped habit with triplanar faceted ends, have been obtained in the presence of inorganic ions (Mg^{2+} and Co^{2+}),[21] small organic molecules,[22] biopolymers,[23] synthetic polymers[20,24] and in some gel systems.[25] Especially, such shapes can be obtained by using biopolymers extracted from sea-urchin spines and nacre proteins. Moreover, the crystal morphology has a high degree of similarity to that of biogenic calcite otoconia. Otoconia in mammals, which act as gravity receptor organs in the inner ear, consist of microcrystals joined together by a filamentous organic matrix of glycosylated proteins to form composite crystals.[26] However, little is known about the mechanism of the

otoconial biosynthesis.[27] The study of the $CaCO_3$ crystallization under the control of CG1 may be helpful for studying glycoprotein-mediated mineralization.

The pseudo-dodecahedron structure was further studied by using AFM and HR-TEM (Fig. 3). Fig. 3a shows the AFM image of the upper surface of a typical pseudo-dodecahedron. The rough and curved feature of the coarse face is in line with the SEM observation. It was calculated that particles on the curved surface are about 100 nm in size. Because the particle may be an aggregate of more than one primary particle, the result indicates that the dimension of primary particles is in the nanoscale. Fig. 3b shows a typical TEM image of the dodecahedron. A thin part of the pseudo-dodecahedron shows lattice fringes with spacing of 0.306 nm, corresponding to an interplanar distance of the (104) plane (Fig. 3c). The image also displays interstices embedded in the crystal matrix (as the white arrow shows). Similar defects can be widely observed in the lattice fringe image (Fig. S3†). The existence of the interstices indicates that the crystallization follows an intermediate mesocrystal pathway.[28] Mesocrystals are a special type of colloidal crystals composed of individual crystallographically aligned nanocrystalline building blocks. In the mesocrystals, the nanocrystals are in perfect crystallographic orientation. However, planar stacking defects between the nanocrystals are inevitable and transform into interstices with polymers upon the ripening process.

The FT-IR spectra were also recorded to characterize the rhombohedra, rods and pseudo-dodecahedra (Fig. 4). For each sample, the vibration bands at *ca.* 712 and 874 cm^{-1} can be attributed to the $\nu 4$ and $\nu 2$ modes of calcite CO_3^{2-}. As the polymer concentration increases, a more evident characteristic absorption band in 1654 cm^{-1} which corresponds to the typical amide I band of CG1 in the crystals can be distinguished (as indicated by the blue dashed line). The results suggest that the CG1 have been gradually incorporated into the crystals. The weight amount of polymers included in the crystals was determined by thermalgravimetric analysis (TG). The percent of remained CG1 is calculated to be about 1.68% in the pseudo-dodecahedra sample obtained in 2.0 g L^{-1} polymer solution (Fig. S4†). And lowering the CG1 concentration leads to a lower weight loss, which is consistent with the FT-IR results. The above results reveal that the polymer plays a crucial role in the morphosynthesis of the calcite crystals.

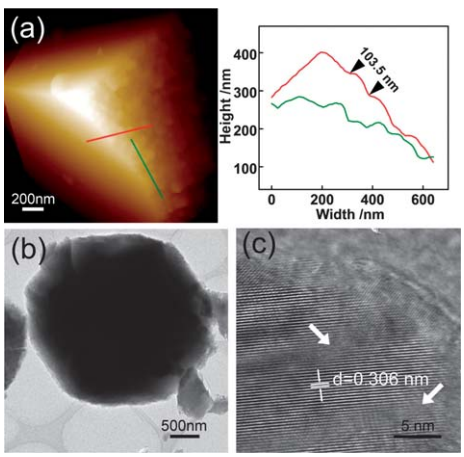

Fig. 3 (a) AFM image of a pseudo-dodecahedral $CaCO_3$ crystal prepared in the polymer solution. (b) TEM image of a pseudo-dodecahedral $CaCO_3$ crystal. (c) HR-TEM image of an ultra thin section of the pseudo-dodecahedral $CaCO_3$ crystal.

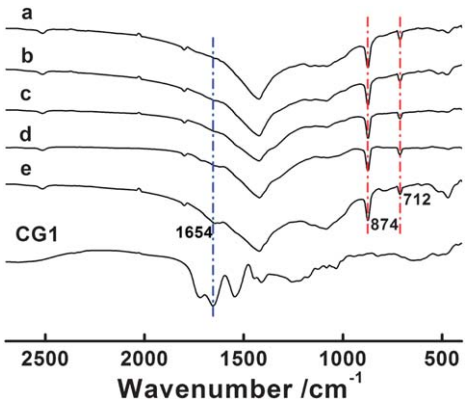

Fig. 4 FT-IR spectra of the CG1 polymer and $CaCO_3$ crystals formed in the polymer solution with various polymer concentrations, (a) 0.01, (b) 0.1, (c) 0.3, (d) 1.0, (e) 2.0 g L^{-1}. The concentration of Ca^{2+} is 2 mM.

The influence of CG2 and CG3 copolymers on $CaCO_3$ crystallization was also studied respectively. Both the CG2 and CG3 copolymers have similar controlling effects to $CaCO_3$ crystallization with CG1 as shown in Fig. S5.† Rod structures were formed in the presence of CG2 and CG3 at a lower concentration (Fig. S5a and S5c†). While in the presence of CG2 and CG3 at a higher concentration, pseudo-dodecahedra were generated (Fig. S5b and S5d†).

3.3 Morphological evolution of $CaCO_3$ mineral with various Ca^{2+} concentrations

In the mineralization, the polymer and Ca^{2+} concentrations are two important factors influencing the final $CaCO_3$ crystal structures. We further investigated the mineralization behavior of $CaCO_3$ crystal at Ca^{2+} concentrations of 1, 3 and 4 mM respectively. At a fixed Ca^{2+} concentration of 1 mM, the $CaCO_3$ morphology changes from rhombohedral structures (Fig. 5a and b) to rods (Fig. 5c) and then to pseudo-dodecahedral structures (Fig. 5d and e) with increasing the polymer concentration. The behavior is similar to that at 2 mM calcium ions (Fig. 2). It is worth noting that the structure displayed in Fig. 5d shows an intermediate morphology between rods and pseudo-dodecahedrons. The structure is oval-shape and has {104} caps at both ends, which suggests a continuous structural transition in the product particles with the variation of copolymer concentration.

Fig. 5f–i display the morphological evolution of $CaCO_3$ crystals at a fixed Ca^{2+} concentration of 4 mM. The crystals show a rhombohedra appearance indicating a less marked influence of polymers at a concentration of 0.001 g L^{-1}. When the polymer concentration was in the range of 0.01 g L^{-1} to 1.0 g L^{-1}, rosette-like spheres were generated which are constructed from

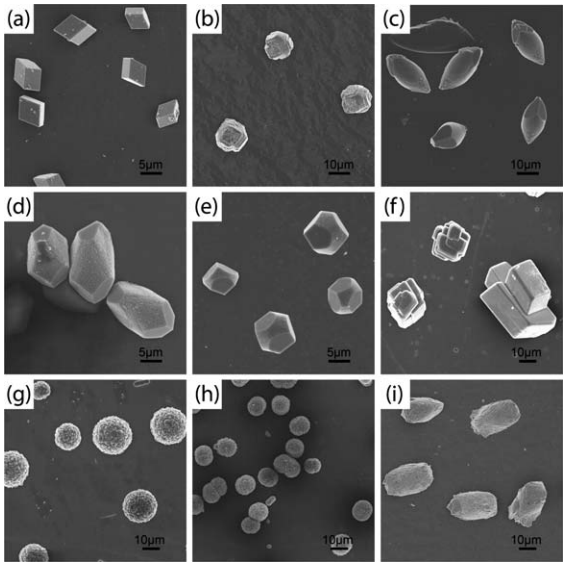

Fig. 5 SEM images of $CaCO_3$ crystals obtained in the presence of CG1 with various of polymer and Ca^{2+} concentrations, (a) [CG1] = 0.001 g L^{-1}, [Ca^{2+}] = 1 mM, (b) [CG1] = 0.003 g L^{-1}, [Ca^{2+}] = 1 mM, (c) [CG1] = 0.1 g L^{-1}, [Ca^{2+}] = 1 mM, (d) [CG1] = 0.3 g L^{-1}, [Ca^{2+}] = 1 mM, (e) [CG1] = 1 g L^{-1}, [Ca^{2+}] = 1 mM, (f) [CG1] = 0.001 g L^{-1}, [Ca^{2+}] = 4 mM, (g) [CG1] = 0.3 g L^{-1}, [Ca^{2+}] = 4 mM, (h) [CG1] = 1.0 g L^{-1}, [Ca^{2+}] = 4 mM, (i) [CG1] = 2.0 g L^{-1}, [Ca^{2+}] = 4 mM.

micrometer crystalline units. In the presence of 2.0 g L^{-1} CG1, rod-shaped calcite crystals were the major product.

The above results indicate that the Ca^{2+} concentration has a remarkable influence on the mineralization behavior. At a fixed polymer concentration of 0.3 g L^{-1}, the morphology of $CaCO_3$ crystals transforms from pseudo-dodecahedrons (Fig. 5d, Ca^{2+} is 1 mM) to rods (Fig. 2d, Ca^{2+} is 2 mM) and then to rosettes (Fig. 5g, Ca^{2+} is 4 mM) with increasing the Ca^{2+} concentration. Since the disorder degree of the arrangement of crystalline units gradually increases with the morphology transformation from pseudo-dodecahedrons to rods and then to rosettes, it can be concluded that a higher Ca^{2+} concentration could lead to a lower efficiency of polymer control action.

The observed structures are summarized in a morphology diagram with respect to the concentration of Ca^{2+} and CG1 (Fig. 6). Each point in the phase diagram corresponds to a mineralization result, and the lines were drawn to identify the resulting morphology boundaries. The morphology diagram is divided into four regions, rhombohedra, rosettes, rods and pseudo-dodecahedrons. At a CG1 polymer concentration below 0.003 g L^{-1}, the copolymers have little effect on the mineralization, leading to the formation of rhombohedra. The etching of the rhombohedra was due to face selective polymer adsorption in a classical growth process in these cases. At a higher Ca^{2+} concentration (above 3 mM) and lower polymer concentration, the crystals exhibit a rosette-like appearance, showing a disordered organization of the building units. In the other two regions, the crystal morphologies are relevant to the concentration ratio of polymer and Ca^{2+}. Rods were formed with lower CG1/Ca^{2+} ratios and pseudo-dodecahedrons were obtained with higher CG1/Ca^{2+} ratios.

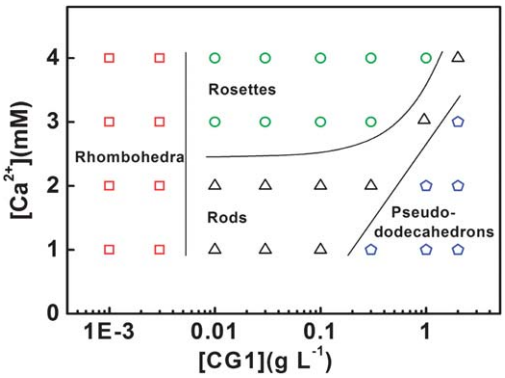

Fig. 6 $CaCO_3$ crystal morphology diagram as functions of Ca^{2+} and polymer concentrations.

3.4 Mechanism study of the β-CD-*b*-PLGA controlled mineralization

The interaction between β-CD-*b*-PLGA and Ca^{2+} was investigated to unveil the mechanism behind the mineralization behavior. A conductivity measurement was applied to verify the interaction between Ca^{2+} and CG1 (Fig. 7).[29] The conductivity of the polymer solution (Λ_{CG1}) and Ca–CG1 hybrid solution (Λ_{Ca-CG1}) was recorded respectively. As the complexion of Ca^{2+} and acidic polymer chains confines the free migration of Ca^{2+}, increase in the polymer concentration makes the value of $\Lambda_{Ca-CG1} - \Lambda_{CG1}$ decrease markedly. For comparison, the conductivity experiments for $PLGA_{99}$ homopolymer and β-CD solution were also carried out respectively. For the $PLGA_{99}$ homopolymer, the changing trend of $\Lambda_{Ca-PLGA} - \Lambda_{PLGA}$ is similar to that observed in CG1/$CaCl_2$ solution. The value of $\Lambda_{Ca-\beta-CD} - \Lambda_{\beta-CD}$ has no obvious fluctuation with the variation of the β-CD concentration, which indicates the β-CD has negligible affinity for Ca^{2+}. The above results indicate that the PLGA block in the copolymer is the functional segment that binds with the Ca^{2+}.

As control experiments, β-CD and $PLGA_{99}$ homopolymers were used individually as additives for modifying $CaCO_3$

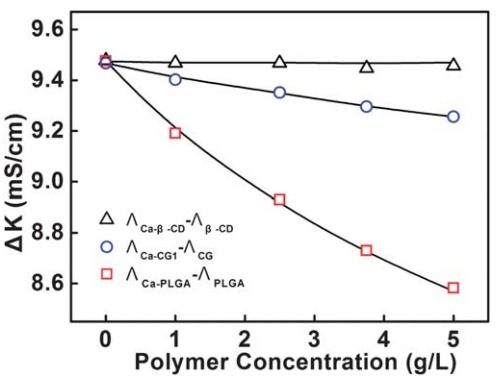

Fig. 7 The conductivity discrepancy curves of the polymer and polymer–$CaCl_2$ hybrid systems as a function of polymer concentration. The $\Lambda_{\beta-CD}$, Λ_{CG1} and Λ_{PLGA} are conductivities of β-CD, CG1 and PLGA. The $\Lambda_{Ca-\beta-CD}$, Λ_{Ca-CG1} and $\Lambda_{Ca-PLGA}$ are conductivities of β-CD, CG1 and PLGA in the presence of 50 mM Ca^{2+}.

mineralization (Fig. S6†). In the case of β-CD, rhombohedral calcite was obtained with the β-CD concentration ranging from 0.01 to 5.0 g L^{-1} (see Fig. S6a†). The morphology appears to be identical to that prepared in the absence of additives. In the case of $PLGA_{99}$, most of the formed crystals are calcite rods at a polymer concentration of 2.0 g L^{-1}, as shown in Fig. S6b (see ESI†). The above results certify that the PLGA segment is a binding block, while the β-CD is a solvating block. On the other hand, the β-CD component plays a significant role in the morphosynthesis of the minerals as indicated by the difference of PLGA and CG1 controlled mineralization.

The time-dependent growth of pseudo-dodecahedra calcite was studied for the mineralization system with 2.0 g L^{-1} polymer and 2 mM Ca^{2+}. The evolution of $CaCO_3$ morphologies at various intervals is shown in Fig. 8. After 2 h reaction, the agglomeration of particles was identified from SEM observation (Fig. 8a). TEM and SAED studies show that these particles were in an amorphous state (Fig. 8b). After mineralization for 5 hours, the amorphous calcium carbonate (ACC) particles tended to aggregate with increasing population, building larger aggregates (Fig. 8c). Over time the aggregates exhibited some crystal faces, indicating that the subunits which are transformed from ACC particles could regulate their positions and self-assemble into oriented aggregation (Fig. 8d). With more ACC particles coalescing into the aggregates and transforming to calcite, a much larger crystal which exposed some crystal faces was obtained at 14 hours (Fig. 8e). After 24 hours of reaction, the morphology is mainly pseudo-dodecahedral calcite and does not change obviously after more time (Fig. 8f).

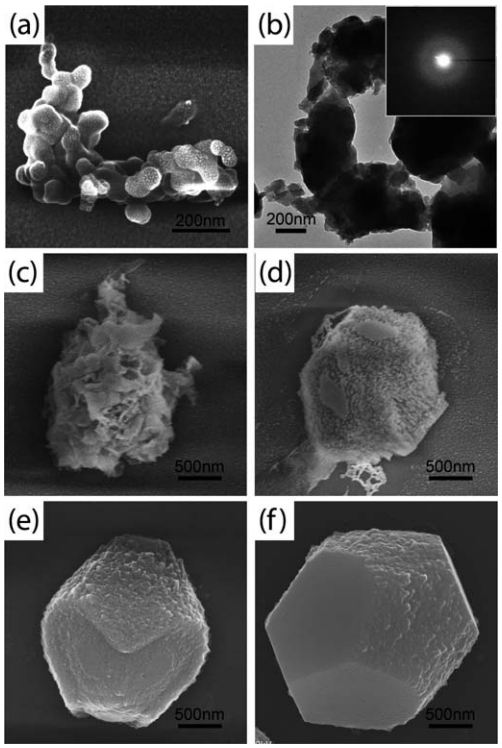

Fig. 8 The morphology evolution of pseudo-dodecahedral calcite crystals. (a) SEM image of particle aggregates for 2 h reaction. (b) TEM image of the particle aggregates and the inset is the SAED pattern of the aggregates. SEM image of $CaCO_3$ sample for various times of reaction, (c) 5 h; (d) 9 h; (e) 14 h; (f) 24 h.

Based on the above analysis, a possible formation mechanism for the $CaCO_3$ crystals is proposed as displayed in Scheme 2. At the beginning, the solution contains complexes of polymers and calcium ions due to the binding interactions between carboxyl groups and calcium ions. Meanwhile, the β-CD serves as a solvating segment because the hydroxyl groups of β-CD cannot attract Ca^{2+} efficiently. In the early stage, the mineralization of $CaCO_3$ is initialized by the decomposition of ammonium carbonate and subsequent diffusion of the CO_2 into the solution (Scheme 2a). ACC particles were deposited as a kinetic product and transiently stabilized by the β-CD-*b*-PLGA for the carboxyl groups.[30] And the ACC particles tended to conglomerate due to van der Waals forces (Scheme 2b). After that, the crystallization of calcite occurs in the ACC particles because of the instability of ACC. As discussed above, the copolymer prefers to adsorb to {*hk*0} faces (Scheme 2c). The β-CD can trap surrounding water molecules within its hydrophobic cavity and in the hydration shell, leading to a volume occupancy of the β-CD segments with surrounding water molecules on the faces.[31] And thus the calcite units are limited to orienting along the crystallographic *c*-axis and fuse together to minimize energy, resulting in the formation of elongated rods with a lower ratio of CG1/Ca^{2+} (Scheme 2e). At a higher calcium ion concentration, the supersaturation of $CaCO_3$ is much higher and thus aggregation of the subunits proceeds rapidly with either no or a low degree of orientation. The poorly controlled process leads to rosette-like crystal formation (Scheme 2f).

While in the case of a higher ratio of β-CD-*b*-PLGA/Ca^{2+}, other crystal faces of a calcite unit may also be covered with extended β-CD segments (Scheme 2d). The dominant growth along the *c*-axis is partly suppressed and {104} faces with lowest energy are well expressed at tip of rods again, resulting in the formation of otoconia crystals (Scheme 2g).

The polymers influence the crystallization process in every period including nucleation, growth and aggregation. In the present study, the presence of amorphous precursors in the initial stage indicates a nucleation inhibition by the β-CD-*b*-PLGA copolymers, which results from the strong interaction between Ca^{2+} and COO^-. In the crystal growth process, the polymers adsorb on the surface of crystals and prevent the further growth along specific crystal faces. On the other hand,

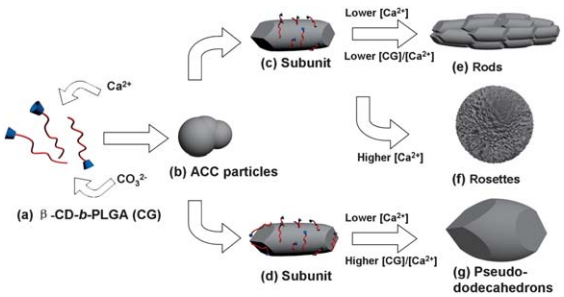

Scheme 2 Scheme showing the growth mechanism of the $CaCO_3$ crystals.

the polymers can decrease the free Ca^{2+} concentration and thus reduce the rate of ionic growth because of the complex formation. A high β-CD-*b*-PLGA concentration leads to a slow nucleation and growth speed, which is favorable for the reorganization of the building units. It can be inferred that the slow nucleation, slow growth and well-organized aggregation are important factors for the formation of pseudo-dodecahedral crystals in a high polymer concentration.

Compared with glycoproteins, the β-CD-*b*-PLGA has a definite chemical structure and mediates a glycoprotein-like mineralization behavior of $CaCO_3$. Therefore, the present work provides a simple method to explore the fundamental mechanism of glycoprotein controlled mineralization. The crystallization pathway *via* the transient ACC and meso-scale assembly was also found in a ovalbumin-controlled $CaCO_3$ mineralization (ovalbumin is a kind of glycoprotein found in egg white), implying that similar pattern may widely exist in glycoprotein-mediated biomineralization.[32] From the experiments, we learned that both the β-CD and PLGA segments play important roles in the morphosynthesis of $CaCO_3$. The results agree with the findings that both polysaccharide and peptide moieties are involved in controlling aspects of crystal growth.[8–10] The function of the acidic polypeptide is to bind specific crystal faces, while the β-CD can adjust the interactions among the primary $CaCO_3$ subunits. Such a strategy may widely exist in glycoprotein-controlled mineralization, in which one part of the polymer selectively adsorbs on specific crystal faces and other part regulates the crystal orientation.[9]

4 Conclusions

In summary, a novel glycoprotein-like copolymer β-CD-*b*-PLGA was prepared and applied for the calcium carbonate mineralization. By adjusting the Ca^{2+} and β-CD-*b*-PLGA concentrations, structures including rosettes, rods, and pseudo-dodecahedrons can be controllably prepared. Both the β-CD and PLGA segments are essential for the mineralization behavior. The formation process is identified to be relevant to a non-classical process by directed aggregation of initially stabilized nanoparticles. In the process, ACC was formed initially and crystallized to subunits subsequently. The final crystals morphology is determined by the meso-scale assembly of the polymer coated subunits. The study offers a simple way to mimic glycoprotein-controlled mineralization and helps to explore the fundamental mechanism in biomineralization.

Acknowledgements

This work was supported by National Natural Science Foundation of China (50925308, 21234002), Key Grant Project of Ministry of Education (313020) and National Basic Research Program of China (no. 2012CB933600). Support from project of Shanghai municipality (10GG15) is also appreciated.

Notes and references

1 S. Mann, *Biomineralization: Principles and Concepts in Bioinorganic Materials Chemistry*, Oxford University Press, Oxford, 2001; A. Dey, G. de With and N. A. J. M. Sommerdijk, *Chem. Soc. Rev.*, 2010, **39**, 397; S. Albeck, J. Aizenberg, L. Addadi and S. Weiner, *J. Am. Chem. Soc.*, 1993, **115**, 11691.
2 A. W. Xu, Y. Ma and H. Cölfen, *J. Mater. Chem.*, 2007, **17**, 415.
3 T. Wang, R. Che, W. Li, R. Mi and Z. Shao, *Cryst. Growth Des.*, 2011, **11**, 2164; W. Li, S. Sun, Q. Yu and P. Wu, *Cryst. Growth Des.*, 2010, **10**, 2685; C. E. Killian, R. A. Metzler, Y. Gong, T. H. Churchill, I. C. Olson, V. Trubetskoy, M. B. Christensen, J. H. Fournelle, F. De Carlo, S. Cohen, J. Mahamid, A. Scholl, A. Young, A. Doran, F. H. Wilt, S. N. Coppersmith and P. U. P. A. Gilbert, *Adv. Funct. Mater.*, 2011, **21**, 682; F. C. Meldrum and H. Cölfen, *Chem. Rev.*, 2008, **108**, 4332.
4 S. Weiner and L. Addadi, *J. Mater. Chem.*, 1997, **7**, 689; K. Benzerara, N. Menguy, P. López-García, T.-H. Yoon, J. Kazmierczak, T. Tyliszczak, F. Guyot and G. E. Brown, *Proc. Natl. Acad. Sci. U. S. A.*, 2006, **103**, 9440; C. Söllner, M. Burghammer, E. Busch-Nentwich, J. Berger, H. Schwarz, C. Riekel and T. Nicolson, *Science*, 2003, **302**, 282; D. Ren, Q. Feng and X. Bourrat, *Micron*, 2011, **42**, 228.
5 G. Falini, S. Albeck, S. Weiner and L. Addadi, *Science*, 1996, **271**, 67; G. He, T. Dahl, A. Veis and A. George, *Nat. Mater.*, 2003, **2**, 552; L. Addadi, D. Joester, F. Nudelman and S. Weiner, *Chem.–Eur. J.*, 2006, **12**, 980; A. A. LinŠ-Krogis, *Acta Zool.*, 1958, **39**, 19; J. L. Arias and M. S. Fernandez, *Chem. Rev.*, 2008, **108**, 4475; K. Henriksen, S. L. S. Stipp, J. R. Young and M. E. Marsh, *Am. Mineral.*, 2004, **89**, 1709.
6 G. Wang, L. Li, J. Lan, L. Chen and J. You, *J. Mater. Chem.*, 2008, **18**, 2789.
7 A. Natoli, M. Wiens, H.-C. Schröder, M. Stifanic, R. Batel, A. L. Soldati, D. E. Jacob and W. E. G. Müller, *Micron*, 2010, **41**, 359.
8 H. Tohse, K. Saruwatari, T. Kogure, H. Nagasawa and Y. Takagi, *Cryst. Growth Des.*, 2009, **9**, 4897.
9 S. Albeck, S. Weiner and L. Addadi, *Chem.–Eur. J.*, 1996, **2**, 278.
10 C. R. MacKenzie, S. M. Wilbanks and K. M. McGrath, *J. Mater. Chem.*, 2004, **14**, 1238.
11 M. F. Butler, N. Glaser, A. C. Weaver, M. Kirkland and M. Heppenstall-Butler, *Cryst. Growth Des.*, 2006, **6**, 781; B. Leng, F. Jiang, K. Lu, W. Ming and Z. Shao, *CrystEngComm*, 2010, **12**, 730.
12 N. Hadjichristidis, H. Iatrou, M. Pitsikalis and J. Mays, *Prog. Polym. Sci.*, 2006, **31**, 1068; L. A. Gower and D. A. Tirrell, *J. Cryst. Growth*, 1998, **191**, 153; P. Kasparov, M. Antonietti and H. Cöfen, *Colloids Surf., A*, 2004, **250**, 153; X. H. Guo, S. H. Yu and G. B. Cai, *Angew. Chem., Int. Ed.*, 2006, **45**, 3977; X. H. Guo, A. W. Xu and S. H. Yu, *Cryst. Growth Des.*, 2008, **8**, 1233.
13 X. Guo, L. Liu, W. Wang, J. Zhang, Y. Wang and S. H. Yu, *CrystEngComm*, 2011, **13**, 2054.
14 W. Zhu, J. Lin and C. Cai, *J. Mater. Chem.*, 2012, **22**, 3939.
15 W. Zhu, C. Cai, J. Lin, L. Wang, L. Chen and Z. Zhuang, *Chem. Commun.*, 2012, **48**, 8544.
16 E. R. Blout and R. H. Karlson, *J. Am. Chem. Soc.*, 1956, **78**, 941; C. Cai, L. Zhang, J. Lin and L. Wang, *J. Phys. Chem. B*, 2008, **112**, 12666.

17 R. C. Petter, J. S. Salek, C. T. Sikorski, G. Kumaravel and F. T. Lin, *J. Am. Chem. Soc.*, 1990, **112**, 3860; Q. Wu, F. Liang, T. Wei, X. Song, D. Liu and G. Zhang, *J. Polym. Res.*, 2010, **17**, 183.
18 R. P. Bonomo, V. Cucinotta, F. D. Allessandro, G. Impellizzeri, G. Maccarrone, E. Rizzarelli and G. Vecchio, *J. Inclusion Phenom. Mol. Recognit. Chem.*, 1993, **15**, 167.
19 L. Addadi and S. Weiner, *Proc. Natl. Acad. Sci. U. S. A.*, 1985, **82**, 4110; L. Addadi, J. Moradian, E. Shay, N. G. Maroudas and S. Weiner, *Proc. Natl. Acad. Sci. U. S. A.*, 1987, **84**, 2732.
20 R. Q. Song, H. Cölfen, A. W. Xu, J. Hartmann and M. Antonietti, *ACS Nano*, 2009, **3**, 1966.
21 A. L. Braybrook, B. R. Heywood, R. A. Jackson and K. Pitt, *J. Cryst. Growth*, 2002, **243**, 336.
22 J. J. De Yoreo and P. M. Dove, *Science*, 2004, **306**, 1301.
23 C. Jimenez-Lopez, A. Rodriguez-Navarro, J. M. Dominguez-Vera and J. M. Garcia-Ruiz, *Geochim. Cosmochim. Acta*, 2003, **67**, 1667; G. Fu, S. Valiyaveettil, B. Wopenka and D. E. Morse, *Biomacromolecules*, 2005, **6**, 1289.
24 R. Q. Song, A. W. Xu, M. Antonietti and H. Cölfen, *Angew. Chem., Int. Ed.*, 2009, **48**, 395.
25 Y. X. Huang, J. Buder, R. Cardoso-Gil, Y. Prots, W. Carrillo-Cabrera, P. Simon and R. Kniep, *Angew. Chem., Int. Ed.*, 2008, **47**, 8280.
26 K. G. Pote and M. D. Ross, *J. Ultrastruct. Mol. Struct. Res.*, 1986, **95**, 61; Y. W. Lundberg, X. Zhao and E. N. Yamoah, *Brain Res.*, 2006, **1091**, 47.
27 Y. Wang, P. E. Kowalski, I. Thalmann, D. M. Ornitz, D. L. Mager and R. Thalmann, *Proc. Natl. Acad. Sci. U. S. A.*, 1998, **95**, 15345.
28 H. Cölfen and S. Mann, *Angew. Chem., Int. Ed.*, 2003, **42**, 2350; H. Cölfen and M. Antonietti, *Angew. Chem., Int. Ed.*, 2005, **44**, 5576; Y. Oaki, A. Kotachi, T. Miura and H. Imai, *Adv. Funct. Mater.*, 2006, **16**, 1633.
29 Z. Chen, C. Wang, H. Zhou and X. Li, *Cryst. Growth Des.*, 2010, **10**, 4722.
30 K. Naka, S. C. Huang and Y. Chujo, *Langmuir*, 2006, **22**, 7760; C. Zhong and C. C. Chu, *J. Mater. Chem.*, 2012, **22**, 6080.
31 W. Saenger, J. Jacob, K. Gessler, T. Steiner, D. Hoffmann, H. Sanbe, K. Koizumi, S. M. Smith and T. Takaha, *Chem. Rev.*, 1998, **98**, 1787.
32 X. Wang, C. Wu, K. Tao, K. Zhao, J. Wang, H. Xu, D. Xia, H. Shan and J. R. Lu, *J. Phys. Chem. B*, 2010, **114**, 5301.